

# The $^{15}\text{N}(\alpha,\gamma)^{19}\text{F}$ reaction and nucleosynthesis of $^{19}\text{F}$

S. Wilmes,\* V. Wilmes,† and G. Staudt

*Physikalisches Institut, Universität Tübingen, Auf der Morgenstelle 14, D-72076 Tübingen, Germany*

P. Mohr‡

*Institut für Kernphysik, Technische Universität Darmstadt,  
Schlossgartenstraße 9, D-64289 Darmstadt, Germany*

J. W. Hammer

*Institut für Strahlenphysik, Universität Stuttgart, Allmandring 3, D-70569 Stuttgart, Germany*

(Dated: November 3, 2018)

Several resonances in the  $^{15}\text{N}(\alpha,\gamma)^{19}\text{F}$  reaction have been investigated in the energy range between 0.6 MeV and 2.7 MeV. Resonance strengths and branching ratios have been determined. High sensitivity could be obtained by the combination of the DYNAMITRON high current accelerator, the windowless gas target system RHINOCEROS, and actively shielded germanium detectors. Two levels of  $^{19}\text{F}$  could be observed for the first time in the  $(\alpha,\gamma)$  channel, and several weak branchings below the detection limits of previous experiments were measured. Two observed resonances correspond to  $\alpha$ -cluster states in  $^{19}\text{F}$  which have been assigned unambiguously. The astrophysical reaction rate is derived from this set of resonance strengths.

PACS numbers: 25.55.-e, 26.20.+f, 26.45.+h

## I. INTRODUCTION

Light nuclei are mainly synthesized by fusion reactions between charged particles. Obvious exceptions are  $^6,7\text{Li}$ ,  $^9\text{Be}$ , and  $^{10,11}\text{B}$ , which are bypassed by the triple-alpha process  $3\alpha \rightarrow ^{12}\text{C}$  and are thus not produced in stellar hydrogen or helium burning. The nucleus  $^{19}\text{F}$  may be produced in a sidepath of the CNO cycle. However, because of the large cross section of the  $^{19}\text{F}(\text{p},\alpha)^{16}\text{O}$  reaction, the freshly synthesized  $^{19}\text{F}$  is destroyed rapidly in any proton-rich environment. As an alternative, the reaction  $^{15}\text{N}(\alpha,\gamma)^{19}\text{F}$  has been suggested as the main production reaction, and the astrophysical scenario is assumed to be a thermally pulsing AGB star [1, 2], and also Wolf-Rayet stars have been suggested [3]. A further possible mechanism for  $^{19}\text{F}$  production is neutrino-induced nucleosynthesis by  $^{20}\text{Ne}(\nu,\nu'\text{N})$  reactions in supernovae [4].

The dominating reaction path for the production of  $^{19}\text{F}$  in AGB stars is assumed to be  $^{14}\text{N}(\alpha,\gamma)^{18}\text{F}(\beta^+)^{18}\text{O}(\text{p},\alpha)^{15}\text{N}(\alpha,\gamma)^{19}\text{F}$  [1, 2]. Destruction of  $^{19}\text{F}$  in a hydrogen-poor environment may proceed via  $^{19}\text{F}(\alpha,\text{p})^{22}\text{Ne}$  which has been studied recently [5]. Typical temperatures are of the order of  $T_9 = 0.2 - 0.3$  (where  $T_9$  is the temperature in  $10^9$  K) which corresponds to effective energies around 350 – 500 keV.

Additional astrophysical interest in the  $^{15}\text{N}(\alpha,\gamma)^{19}\text{F}$  reaction comes from the fact that properties of the  $^{19}\text{Ne}$  mirror nucleus can be derived assuming similar reduced

widths  $\theta_\alpha^2$  and radiation widths  $\Gamma_\gamma$ . The  $^{15}\text{O}(\alpha,\gamma)^{19}\text{Ne}$  reaction is the bottleneck for the outbreak from the hot CNO cycle to the rapid proton capture process [6, 7], and therefore reduced widths  $\theta_\alpha^2$  have to be determined for the first states above the  $\alpha$  threshold in  $^{19}\text{Ne}$ . Additionally, higher-lying resonances in  $^{15}\text{N}(\alpha,\gamma)^{19}\text{F}$  have been studied [8] which correspond to the lowest resonances in the  $^{18}\text{F}(\text{p},\alpha)^{15}\text{O}$  and  $^{18}\text{F}(\text{p},\gamma)^{19}\text{Ne}$  reactions. Any direct experimental study of the latter reactions is hampered by the unstable nuclei  $^{15}\text{O}$  and  $^{18}\text{F}$ . However, there are significant uncertainties in the translation of properties of  $^{19}\text{F}$  to its mirror nucleus  $^{19}\text{Ne}$  which may lead to uncertainties up to more than one order of magnitude for the corresponding reaction rates [9].

The astrophysical reaction rate of  $^{15}\text{N}(\alpha,\gamma)^{19}\text{F}$  is dominated by resonance contributions of several low-lying states in  $^{19}\text{F}$ . Several  $(\alpha,\gamma)$  experiments on individual resonances have been performed, but no previous experiment has covered a broad energy range from several hundred keV up to a few MeV [10, 11, 12, 13, 14, 15, 16]. The available information is summarized in [17, 18, 19]. This paper presents new experimental data in the energy range from 0.6 MeV to 2.7 MeV. All data have been measured with the same set-up; this leads to a complete and consistent set of resonance strengths. With the exception of the  $7/2^+$  resonance at 461 keV all astrophysically relevant resonance strengths could be determined. The strength of this resonance was measured indirectly in an  $\alpha$ -transfer experiment using the  $^{15}\text{N}(^7\text{Li},\text{t})^{19}\text{F}$  reaction [20]. The lowest resonance with  $J^\pi = 9/2^-$  at  $E_x = 4033$  keV ( $E_\alpha = 24$  keV) does not contribute significantly to the reaction rate at the given temperatures.

The paper is organized as follows: In Sect. II we present briefly our experimental set-up. Results for the resonance strengths and the branching ratios are given in

\*Allianz Vers. AG, Königinstraße 28, D-80802 München, Germany

†Mädchenrealschule Weichs, Freiherrnstraße 17, D-85258 Weichs, Germany

‡Corresponding Author; E-mail: mohr@ikp.tu-darmstadt.de

Sect. III.  $\alpha$ -cluster states in  $^{19}\text{F}$  are discussed in Sect. IV. The astrophysical reaction rate is calculated in Sect. V, and finally conclusions are drawn in Sect. VI.

In this paper energies  $E_\alpha$  are given in the laboratory system. The center-of-mass energy  $E_{c.m.}$  is related to  $E_\alpha$  and to the excitation energy  $E_x$  by the well-known formulae  $E_{c.m.} = E_\alpha \times A_T / (A_P + A_T) \approx 0.7894 E_\alpha$  and  $E_x = E_{c.m.} + Q$  with  $Q = 4013.8 \text{ keV}$ .

## II. EXPERIMENTAL SET-UP

The experiment has been performed at the windowless gas target system RHINOCEROS [21] which is installed at the DYNAMITRON accelerator of Universität Stuttgart. Details of the experimental set-up and the data analysis are given in [22, 23]. Here we repeat briefly the relevant properties of this set-up.

The  $^4\text{He}^+$  beam with currents up to  $120 \mu\text{A}$  was focussed into an extended windowless gas target area with a length of about 6 cm. The  $\text{N}_2$  target gas was highly enriched in  $^{15}\text{N}$  to 98% and 99.7%. The gas was recirculated and purified by a cooling trap. Typical target pressures were about 1 mbar. Two diaphragms with a length of 15 mm and a diameter of 5 mm were used to collimate the  $\alpha$  beam and to define the target area. Several additional diaphragms had to be used to reduce the pressure by 8 orders of magnitude to the vacuum in the beam transport system of  $10^{-8}$  mbar. The windowless gas target system has the advantages of high stability (it cannot be damaged by the beam), of high purity and of variable density which can be easily changed by the target pressure.

The  $\alpha$ -beam was monitored by two silicon surface-barrier detectors mounted either at  $27.5^\circ$ ,  $60^\circ$ , or  $90^\circ$  relative to the  $\alpha$  beam axis. The positions of the particle detectors were chosen to obtain small deviations from the Rutherford cross section at reasonable counting rates.

For the detection of the  $\gamma$ -rays we used two large-volume high-purity germanium (HPGe) detectors with efficiencies up to about 100% (relative to a  $3'' \times 3''$  NaI(Tl) detector). One detector was actively shielded by a BGO detector. The efficiency determination of the HPGe detectors was obtained from GEANT simulations which were shown to be reliable in the analyzed energy region [22]. For a reliable determination of weak branching ratios we have taken into account summing effects from cascade  $\gamma$ -rays.

Typical spectra are shown in Figs. 1 and 2. Fig. 1 shows a spectrum of the silicon detector mounted at  $\vartheta_{\text{lab}} = 27.5^\circ$ , and Fig. 2 presents a  $\gamma$ -ray spectrum of the HPGe detector in the  $1/2^+$  resonance at  $E_x = 5337 \text{ keV}$ .

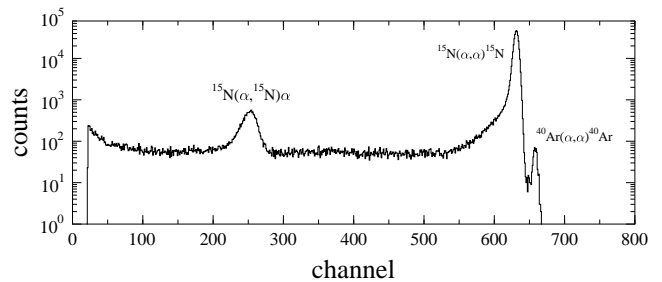


FIG. 1: Energy spectrum of the particle detector mounted at  $\vartheta_{\text{lab}} = 27.5^\circ$ . Besides the dominating peak from  $^{15}\text{N}(\alpha, \alpha)^{15}\text{N}$  also the recoil nucleus  $^{15}\text{N}$  is clearly visible. Additionally, a weak contamination of the target gas ( $^{40}\text{Ar}$ ;  $\approx 0.015\%$ ) can be seen. The spectrum has been measured at  $E_\alpha = 1640 \text{ keV}$ .

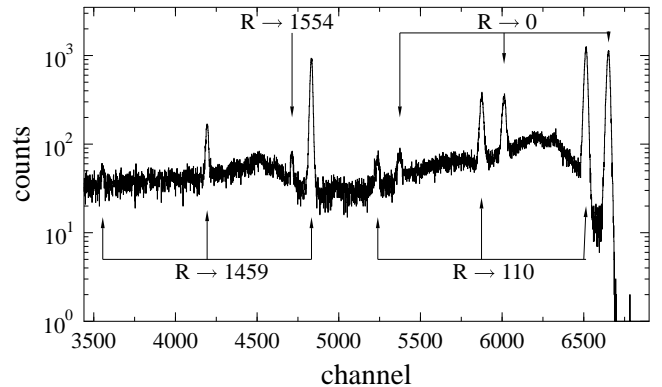


FIG. 2: Energy spectrum of the HPGe detector, measured at the  $1/2^+$  resonance at  $E_x = 5337 \text{ keV}$  ( $E_\alpha = 1676 \text{ keV}$ ). Transitions to the final states at  $E_x = 0, 110, 1459$ , and  $1554 \text{ keV}$  can be seen. The corresponding full energy, single escape, and double escape peaks are marked. This spectrum has been measured in anticoincidence with the signal from the active BGO shielding.

## III. RESONANCE STRENGTHS AND BRANCHING RATIOS

The resonance strength  $\omega\gamma$  of a resonance is defined by

$$\omega\gamma = \omega \frac{\Gamma_\alpha \Gamma_\gamma}{\Gamma} \quad (1)$$

with a statistical factor  $\omega = (2J + 1) / [(2J_P + 1)(2J_T + 1)] = (2J + 1) / 2$  for  $^{15}\text{N}(\alpha, \gamma)^{19}\text{F}$  and the partial widths  $\Gamma_\alpha$ ,  $\Gamma_\gamma$ , and the total width  $\Gamma = \Gamma_\alpha + \Gamma_\gamma$  for excitation energies below other particle thresholds of  $^{19}\text{F}$  ( $S_n = 10432 \text{ keV}$ ,  $S_p = 7994 \text{ keV}$ ). The resonance strength is approximately given by  $\omega\gamma \approx \omega\Gamma_\alpha$  for  $\Gamma_\alpha \ll \Gamma_\gamma$  and  $\omega\gamma \approx \omega\Gamma_\gamma$  for  $\Gamma_\gamma \ll \Gamma_\alpha$ . The first case is expected for resonances close above the  $\alpha$  threshold at  $4014 \text{ keV}$  whereas the second case can be found at higher energies. For several states the ratio  $\Gamma_\gamma / \Gamma$  has been measured where the  $^{12}\text{C}(^{11}\text{B}, \alpha)^{19}\text{F}$  reaction has been used for the population of these states [24].

The resonance strength  $\omega\gamma$  is related to the experimen-

tal yield  $Y$  by

$$Y = \frac{N_P \rho_T}{S} \frac{A_P + A_T}{A_T} \frac{\pi^2 \hbar^2}{\mu E_{c.m.}} (\omega \gamma) \quad (2)$$

with the number of projectiles  $N_P$ , the density of target atoms  $\rho_T$  (in  $\text{cm}^{-3}$ ), the stopping power  $S$  (in  $\text{keV}/\mu\text{m}$ ), and the reduced mass  $\mu$ . Resonance strengths and branching ratios for all measured resonances have been determined by the following procedure: The product of the number of projectiles and target atoms per  $\text{cm}^2$  was derived from the elastically scattered  $\alpha$  particles in the silicon detectors. Using the geometry of the particle detectors, the product of the number of projectiles  $N_P$  and the target density  $\rho_T$  is calculated. The elastic cross section was assumed to follow Rutherford's law for pointlike charges. This assumption was tested by an additional measurement using a different target chamber with three silicon detectors at  $\vartheta_{\text{lab}} = 30^\circ$ ,  $60^\circ$ , and  $135^\circ$ , and a mixture of xenon and  $^{15}\text{N}$  as target gas. As can be seen from Fig. 3, the deviations for the most forward detector are very small and remain within about 10% even for the broad resonances at  $E_\alpha = 1676$ ,  $1884$ , and  $2627$  keV. These deviations have been taken into account for the determination of the strengths of the mentioned resonances. The stopping power  $S$  was taken from [25]. The energies of the resonances were taken from [18]; all energies were confirmed within their uncertainties by the measured  $\gamma$ -ray energies.

The number of reactions was determined from the number of counts in the peaks of the HPGe  $\gamma$ -ray spectra. The efficiency of the HPGe detectors was calculated by GEANT simulations which were verified by measurements with radioactive sources and by the analysis of the  $^{27}\text{Al}(p,\gamma)^{28}\text{Si}$  reaction [22]. The angular distribution of the  $\gamma$ -rays was taken into account. We assumed pure  $E1$  transitions for  $\Delta I = 0, \pm 1$ ,  $\pi = -1$ ; for  $\Delta I = 0, \pm 1$ ,  $\pi = +1$  we calculated  $M1/E2$  angular distributions with a mixing parameter  $\delta$  from [18] whenever available or  $\delta = 0$  otherwise; for  $\Delta I = 2$ ,  $\pi = +1$  pure  $E2$  radiation is assumed. The close geometry of the HPGe detector with a distance of only 6 cm leads to a large coverage of  $60^\circ \leq \vartheta_\gamma \leq 120^\circ$ . Because of the half-integer spin of  $^{15}\text{N}$  the deviations from an isotropic angular distribution are much smaller compared to spin-zero target nuclei, e.g. in the reaction  $^{20}\text{Ne}(\alpha,\gamma)^{24}\text{Mg}$ , see [22]. Therefore, the uncertainties remain small even in cases where  $\delta$  is unknown.

The overall uncertainties are dominated by the efficiency determination ( $\lesssim 4\%$ ), the density profile of the target gas (mainly for broad resonances,  $\lesssim 5\%$ ), the stopping power ( $\lesssim 5\%$ ), in rare cases by the unknown mixing parameter ( $\lesssim 10\%$ ), and sometimes by poor statistics. The sizes of these uncertainties change from transition to transition. The given values are typical leading to overall uncertainties of the resonance strengths of  $\lesssim 10\%$  and much smaller uncertainties of the branching ratios.

The results for the resonance strengths are compared to literature values in Table I. The measured branching

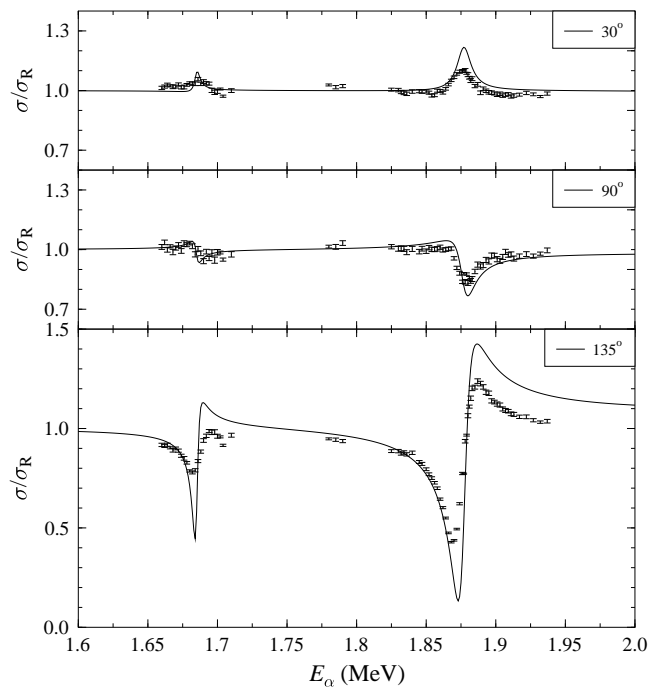


FIG. 3: Elastic scattering cross sections around the  $J^\pi = 1/2^+$ ,  $E_x = 5337$  keV and  $J^\pi = 3/2^+$ ,  $E_x = 5501$  keV resonances, normalized to Rutherford cross section, measured with silicon detectors at  $\vartheta_{\text{lab}} = 30^\circ$  (upper diagram),  $60^\circ$  (middle), and  $135^\circ$  (lower). The full line is an optical model calculation (see Sect. IV).

ratios are listed in Table II. In the following paragraphs further information is given on all resonances.

#### A. $J^\pi = 9/2^-$ , $E_x = 4033$ keV and $J^\pi = 7/2^+$ , $E_x = 4378$ keV and $J^\pi = 13/2^+$ , $E_x = 4648$ keV

No attempt was made to measure these three resonances in this experiment. The resonances at 4033 keV and 4648 keV do not significantly contribute to the astrophysical reaction rate. Their strengths are very small because the partial widths  $\Gamma_\alpha$  are suppressed as a consequence of the large centrifugal barrier.

Nevertheless, the astrophysical reaction rate around  $T_9 = 0.1 - 0.2$  is strongly influenced by the resonance at  $E_x = 4378$  keV. The resonance strength of this  $7/2^+$  resonance is entirely determined by its partial width  $\Gamma_\alpha$  which is confirmed by the measured ratio  $\Gamma_\gamma/\Gamma > 0.96$  [24]. The partial width  $\Gamma_\alpha$  has been measured in the  $^{15}\text{N}(^7\text{Li,t})^{19}\text{F}$  reaction:  $\Gamma_\alpha = 1.5_{-0.8}^{+1.5}$  neV [9, 20]. This leads to a resonance strength of  $\omega\gamma = 6_{-3}^{+6}$  neV which is far below our experimental sensitivity of the order of  $1 \mu\text{eV}$ .

TABLE I: Resonance strengths  $\omega\gamma$  for the resonances between  $E_\alpha = 461$  and  $2642$  keV ( $4378$  keV  $\leq E_x \leq 6100$  keV). The results show overall good agreement with the literature data  $\omega\gamma_{\text{Lit}}$  [18]; detailed references are given in the last column. All energies  $E_\alpha$  and  $E_x$  are given in keV.

$E_\alpha$	$E_x$	$J^\pi$	$\omega\gamma^a$	$\omega\gamma_{\text{Lit}}^b$	Ref.
461	4378	$7/2^+$	–	$6^{+6}_{-3}$ neV <sup>c</sup>	[20]
679	4550	$5/2^+$	$(95.5 \pm 11.7)$ $\mu\text{eV}$	$(97 \pm 20)$ $\mu\text{eV}$	[10]
687	4556	$3/2^-$	$(6.4 \pm 2.5)$ $\mu\text{eV}$	$< 10$ $\mu\text{eV}$	[10]
847	4683	$5/2^-$	$(5.6 \pm 0.6)$ meV	$(6 \pm 1)$ meV	[11]
1384	5107	$5/2^+$	$(9.7 \pm 1.6)$ meV	$(13 \pm 8)$ meV	[15, 26]
1676	5337	$1/2^+$	$(1.69 \pm 0.14)$ eV	$(1.64 \pm 0.16)$ eV	[13]
1778	5418	$7/2^-$	$(380 \pm 44)$ meV	$(420 \pm 90)$ meV	[15, 26]
1837	5464	$7/2^+$	$(2.10 \pm 0.14)$ eV	$(2.5 \pm 0.4)$ eV	[14]
1884	5501	$3/2^+$	$(3.56 \pm 0.34)$ eV	$(4.2 \pm 1.1)$ eV	[16, 26]
1927	5535	$5/2^+$	$(344 \pm 40)$ meV	$(480 \pm 110)$ meV	[15, 26]
2036	5621	$5/2^-$	$(323 \pm 38)$ meV	$(370 \pm 90)$ meV	[12]
2437	5938	$1/2^+$	$(416 \pm 48)$ meV	$(530 \pm 130)$ meV	[12]
2604	6070	$7/2^+$	$(2.10 \pm 0.26)$ eV	$(2.7 \pm 0.54)$ eV	[12]
2627	6088	$3/2^-$	$(5.0 \pm 0.6)$ eV	$(4.5 \pm 0.9)$ eV	[12]
2642	6100	$9/2^-$	$(440 \pm 69)$ meV	–	–

<sup>a</sup>this work

<sup>b</sup>Ref. [18]

<sup>c</sup>from  $^{15}\text{N}(^7\text{Li},t)^{19}\text{F}$  transfer experiment [20]

### B. $J^\pi = 5/2^+$ , $E_x = 4550$ keV and $J^\pi = 3/2^-$ , $E_x = 4556$ keV

Both resonances have been discussed in detail in [27]; the experimental thick-target yield is shown in Fig. 2 of [27]. For the lower resonance a weak branch to the ground state has been detected for the first time in the  $(\alpha, \gamma)$  reaction. With the assumption  $\Gamma_\alpha \ll \Gamma_\gamma \approx \Gamma$  and the total width  $\Gamma = 101 \pm 55$  meV from a lifetime measurement [28] one obtains a ground state radiation width  $\Gamma_{\gamma_0} \approx 4$  meV in excellent agreement with the transition strength in [29]:  $B(E2) = 1.0 \pm 0.2$  W.u. corresponding to  $\Gamma_{\gamma_0} = 4.8 \pm 1.0$  meV. The total strength of  $\omega\gamma = 95.5 \pm 11.7$   $\mu\text{eV}$  is in excellent agreement with a previous result [10, 18].

For the very weak resonance at  $E_x = 4556$  keV only the strongest branching to the first excited state at  $E_x = 110$  keV could be detected. Together with the known branching ratio of 45% [18] a resonance strength of  $\omega\gamma = 6.4 \pm 2.5$   $\mu\text{eV}$  was derived. This value agrees with the previously adopted upper limit of  $\omega\gamma \leq 10$   $\mu\text{eV}$  [10].

### C. $J^\pi = 5/2^-$ , $E_x = 4683$ keV

The total strength of this resonance is  $\omega\gamma = 5.6 \pm 0.6$  meV which is in good agreement with the adopted strength of  $\omega\gamma = 6 \pm 1$  meV [11, 18]. Two weak branching ratios to the states at  $E_x = 110$  and  $1554$  keV have been detected for the first time; both branching ratios are close to the upper limits in [18].

### D. $J^\pi = 5/2^+$ , $E_x = 5107$ keV

The total strength of this resonance is  $\omega\gamma = 9.7 \pm 1.6$  meV. The uncertainties have been reduced significantly compared to the adopted value of  $\omega\gamma = 13 \pm 8$  meV [15, 18]. Six branching ratios for this resonance have been confirmed with slightly improved accuracies.

From the measured ratio  $\Gamma_\gamma/\Gamma = 0.97 \pm 0.03$  [24] and our resonance strength one can deduce  $\Gamma_\alpha = 3.3 \pm 0.6$  meV. The measured upper limit of the lifetime leads to a total width  $\Gamma > 22$  meV [18], and thus  $\Gamma_\gamma > 19$  meV for this state.

### E. $J^\pi = 1/2^{(+)}$ , $E_x = 5337$ keV

Spin and parity  $J^\pi = 1/2^{(+)}$  have been adopted in [18]. As we shall show later, there is clear confirmation of the positive parity from our experimental data (see Sect. IV). Therefore, the resonance will be labelled by  $J^\pi = 1/2^+$  in the following discussion.

This resonance allows a precise comparison of this gas target experiment to previous experiments which were performed using solid targets. The previously adopted strength of this resonance of  $\omega\gamma = 1.64 \pm 0.16$  eV [13, 18] has a small uncertainty of about 10%. The resonance is relatively strong and has been seen in several later experiments. Often, this resonance has been used as calibration standard for other resonances (see discussion in [26]). Because of  $J^\pi = 1/2^+$  the angular distribution for all decay  $\gamma$ -rays is isotropic. This leads to small uncertainties for the branching ratios. Within the experimental uncertainties, we confirm the adopted branching ratios [18]. Additionally, two weak decay branchings to states at  $E_x = 1554$  and  $3908$  keV have been observed. Our observed resonance strength  $\omega\gamma = 1.69 \pm 0.14$  eV is 3% higher than the adopted value, but agrees nicely within the uncertainties.

The total width  $\Gamma$  could be determined from the analysis of the measured yield curve over a broad energy interval of about 100 keV following the procedure outlined in [22]. The result of  $\Gamma = 1.3 \pm 0.5$  keV replaces the adopted lower limit  $\Gamma > 6.6$  eV. For this resonance  $\Gamma_\alpha \approx \Gamma$ . This fact is confirmed by the observation of this  $1/2^+$  resonance in the elastic scattering data (see Fig. 3). Thus,  $\Gamma_\gamma = 1.69 \pm 0.14$  eV.

### F. $J^\pi = 7/2^-$ , $E_x = 5418$ keV and $J^\pi = 7/2^+$ , $E_x = 5464$ keV

Because of the relative large  $J = 7/2$  of both resonances, transitions to the ground state and first excited state of  $^{19}\text{F}$  with  $J = 1/2$  are very unlikely. Indeed, no resonant enhancement can be seen in the yield curves. The observed yields are small and can be completely understood as the tails of the broad  $3/2^+$  resonance at  $E_x = 5501$  keV (see Sect. III G and IV). A

TABLE II: Experimentally determined branching ratios (in %) for 14 resonances of the reaction  $^{15}\text{N}(\alpha,\gamma)^{19}\text{F}$  are given (first lines) and compared to literature values (second lines) from [18]. Several new branching ratios have been observed for the first time. The detection limit for weak branchings is typically much smaller than 1%. Spins and parities  $J^\pi$  and excitation energies  $E_x$  have been taken from [18]. All excitation energies are given in keV.

$J^\pi; E_{x,i} \rightarrow$	0	110	197	1346	1459	1554	2780	3908	3999	4033	4378	4550	4556	4683	5107
5/2 <sup>+</sup> ;4550	4.0±2.0	—	69.8±7.2	3.5±1.9	9.7±1.8	12.9±2.0	—	—	—	—	—	—	—	—	—
[18]	< 5 <sup>a</sup>	—	69±7	5±3	8±3	18±4	—	—	—	—	—	—	—	—	—
3/2 <sup>-</sup> ;4556	—	* <sup>b</sup>	—	—	—	—	—	—	—	—	—	—	—	—	—
[18]	36±4	45±5	9±3	4±3	< 4	6±3	—	—	—	—	—	—	—	—	—
5/2 <sup>-</sup> ;4683	—	1.3±0.5	7.7±0.7	62.8±3.0	26.9±1.4	1.4±0.3	—	—	—	—	—	—	—	—	—
[18]	—	< 1.5	5.6±0.9	63.1±3.8	31.3±2.2	< 5	—	—	—	—	—	—	—	—	—
5/2 <sup>+</sup> ;5107	—	—	77.8±3.8	—	8.4±0.6	3.2±0.4	0.7±0.3	6.9 <sup>+0.5</sup> <sub>-1.0</sub>	—	—	3.0±0.3	—	—	—	—
[18]	—	—	79.7±3.7	< 1.6	10.4±2.7	1.8±1.8	0.7±0.6	5.4±0.9	—	—	2.0±0.5	—	—	—	—
1/2 <sup>+</sup> ;5337	38.9±1.0	40.2±1.1	—	—	20.0±0.6	0.8±0.1	—	0.1±0.02	—	—	—	—	—	—	—
[18]	37±4	42±4	—	—	20±2	< 2	—	—	—	—	—	—	—	—	—
7/2 <sup>-</sup> ;5418	—	—	—	72.7±2.8	12.4±0.7	—	—	—	9.3±0.4	5.2±0.3	—	—	—	0.4±0.1	—
[18]	—	—	—	70	13	—	—	—	10	6	—	—	—	—	—
7/2 <sup>+</sup> ;5464	—	—	3.8±0.5	32.5±1.0	—	4.9±0.2	58.1±1.7	—	—	—	0.2±0.03	0.5±0.03	—	—	—
[18]	—	—	4	32	—	5	59	—	—	—	—	—	—	—	—
3/2 <sup>+</sup> ;5501	—	21.0±0.8	49.1±1.7	16.6±0.6	1.5±0.2	11.7±0.5	—	—	—	—	—	—	—	—	—
[18]	—	25	49	16	—	11	—	—	—	—	—	—	—	—	—
5/2 <sup>+</sup> ;5535	6.7±0.4	—	38.6±2.3	—	50.3±2.0	2.0±0.2	—	0.6±0.06	—	—	0.9±0.1	—	0.4±0.08	—	0.5±0.09
[18]	7	—	47	—	45	—	—	—	—	—	—	—	—	—	—
5/2 <sup>-</sup> ;5621	—	—	36.8±2.0	47.8±2.5	4.6±0.4	—	—	—	8.0±0.5	—	—	1.2±0.2	—	1.5±0.2	—
[18]	—	—	39±4	61±4	—	—	—	—	—	—	—	—	—	—	—
1/2 <sup>+</sup> ;5938	5.3±0.3	20.6±0.9	0.9±0.2	—	65.0±2.4	0.4±0.2	—	7.9±0.4	—	—	—	—	—	—	—
[18]	7±4	20±6	2±1	—	63±6	< 2	—	8±3	—	—	—	—	—	—	—
7/2 <sup>+</sup> ;6070	—	—	52.3±2.0	20.6±0.8	—	1.1±0.2	20.9±0.8	—	—	0.1±0.04	4.0±0.2	1.0±0.05	—	—	—
[18]	—	—	54±5	19±2	—	1 <sup>+1</sup> <sub>-0.5</sub>	23±3	—	—	< 1	4±1	—	—	—	—
3/2 <sup>-</sup> ;6088	25.1±1.0	60.3±2.2	14.6±0.6	—	—	—	—	—	—	—	—	—	—	—	—
[18]	25±4	61±5	14±3	—	—	—	—	—	—	—	—	—	—	—	—
9/2 <sup>-</sup> ;6100	—	—	19.4±7.2	11.4±1.6	—	< 4.4	2.9±0.8	—	16.9±1.5	41.1±3.5	8.4±0.8	—	—	—	—
[18]	—	—	—	—	—	—	—	—	—	—	—	—	—	—	—

<sup>a</sup>See Sect. III B and [17].

<sup>b</sup>Observed transition; see Sect. III B.

resonant enhancement was found for 5 transitions in the 5418 keV resonance (including one new weak branching) and for 6 transitions in the 5464 keV resonance (including two new weak branchings). The summed strengths are  $\omega\gamma = 380 \pm 44$  meV for the 5418 keV resonance and  $\omega\gamma = 2.10 \pm 0.14$  eV for the 5464 keV resonance. For both strengths and branching ratios good agreement with the adopted values [14, 15, 18, 26] is found. No uncertainties are given for the adopted branching ratios [18].

For the 5418 keV resonance the ratio  $\Gamma_\gamma/\Gamma = 0.04 \pm 0.007$  has been measured [24] which allows to calculate the partial widths  $\Gamma_\alpha = 2.4 \pm 0.3$  eV and  $\Gamma_\gamma = 98 \pm 12$  meV. This leads to a total width  $\Gamma = 2.5 \pm 0.4$  eV which agrees perfectly with the adopted  $\Gamma = 2.6 \pm 0.7$  eV.

For the 5464 keV resonance only an upper limit  $\Gamma_\gamma/\Gamma < 0.028$  was measured [24] which leads to the partial widths  $\Gamma_\alpha > 18.8$  eV and  $\Gamma_\gamma \approx 525 \pm 35$  meV. For the total width we obtain  $\Gamma > 19.3$  eV, which is not in contradiction with a lifetime measurement of  $\Gamma > 2.5$  eV.

#### G. $J^\pi = 3/2^+$ , $E_x = 5501$ keV

The strength of this relatively broad resonance is  $\omega\gamma = 3.56 \pm 0.34$  eV which is slightly smaller than the adopted value of  $4.2 \pm 1.1$  eV [16, 18, 26]. A correction of 11 % was taken into account because of the deviation of the elastic scattering cross section from Rutherford in this resonance (see Fig. 3 and Sect. IV). Tails of this resonance could be observed over a broad interval of about 400 keV, and from the yield curve a total width of  $\Gamma = 4.7 \pm 1.6$  keV could be derived in the same way as for the 5337 keV resonance (see Sect. III E). This value agrees nicely with the adopted width  $\Gamma = 4 \pm 1$  keV [18].

With the exception of the transition to the first excited state at  $E_x = 110$  keV, all branching ratios agree with the adopted values [18] which are again given without uncertainties. One new branching has been measured to  $E_x = 1459$  keV.

From the resonance strength one can directly calculate the radiation width  $\Gamma_\gamma = 1.78 \pm 0.17$  eV. Because of the large total width one can assume  $\Gamma_\alpha \approx \Gamma$  and therefore  $\Gamma_\alpha \gg \Gamma_\gamma$  for this resonance. This assumption is confirmed by the elastic scattering data (see Sect. IV).

#### H. $J^\pi = 5/2^+$ , $E_x = 5535$ keV and $J^\pi = 5/2^-$ , $E_x = 5621$ keV

Both  $J = 5/2$  resonances lie in the high-energy tail of the broad 5501 keV resonance. Therefore, for several transitions to low-lying states in  $^{19}\text{F}$  a small contribution from the broad 5501 keV resonance has to be subtracted. The summed strengths are  $\omega\gamma = 344 \pm 40$  meV for the 5535 keV resonance and  $\omega\gamma = 323 \pm 38$  meV for the 5621 keV resonance. Both values are in agreement with the adopted values within their large uncertainties.

Eight branching ratios (including five new ones) have been measured for the 5535 keV resonance which are in reasonable agreement with the adopted values [18]. For the 5621 keV resonance six branchings (including four new ones) were measured.

#### I. $J^\pi = 1/2^+$ , $E_x = 5938$ keV

The resonance at  $E_x = 5938$  keV is more than 400 keV above the broad 5501 keV resonance and 150 keV below the broad 6088 keV resonance thus not influenced by their tails. We find a total strength of  $\omega\gamma = 416 \pm 48$  meV slightly lower than the adopted value of  $\omega\gamma = 530 \pm 130$  meV [12, 18]. Six branching ratios were determined including a new weak  $0.4 \pm 0.2\%$  branching to the  $E_x = 1554$  keV state.

#### J. $J^\pi = 3/2^-$ , $E_x = 6070$ keV and $J^\pi = 7/2^+$ , $E_x = 6088$ keV and $J^\pi = 9/2^-$ , $E_x = 6100$ keV

These three resonances are located close to each other, and the central 6088 keV resonance has a rather large width of  $\Gamma = 4$  keV. This value is confirmed by the analysis of our yield curve which leads to  $\Gamma = 4.7 \pm 1.6$  keV. The lower resonance is a factor of four narrower:  $\Gamma = 1.2$  keV, and the width is unknown for the 6100 keV resonance.

From a careful analysis of the yield curves including Doppler shifts in the  $\gamma$  spectra (see also [27]) we are able to disentangle the contributions of these three resonances. Fortunately, these resonances show very different branching ratios which made the analysis less complicated than expected. The total strengths are  $\omega\gamma = 2.1 \pm 0.26$  eV,  $5.0 \pm 0.6$  eV, and  $440 \pm 69$  meV for  $E_x = 6070$  keV, 6088 keV, and 6100 keV. The first two numbers are in good agreement with previous data [12, 18] whereas the resonance at  $E_x = 6100$  keV has been measured for the first time in the  $^{15}\text{N}(\alpha, \gamma)^{19}\text{F}$  reaction. The measured branching ratios agree perfectly with the adopted values for the  $E_x = 6088$  keV resonance; two new branchings have been detected in the  $E_x = 6070$  keV resonance, and no branching ratios are given in [18] for the  $E_x = 6100$  keV resonance.

### IV. $\alpha$ -CLUSTER STATES IN $^{19}\text{F}$ AND DIRECT CAPTURE

$\alpha$  clustering is a well-known phenomenon in light nuclei. Characteristic properties of states with strong  $\alpha$  clustering are large  $\alpha$ -particle spectroscopic factors which can be measured in  $\alpha$  transfer reactions and relatively large partial widths  $\Gamma_\alpha$  for states above threshold. Many properties of  $^{19}\text{F}$  can be understood from such a simple model which neglects excitations in the  $\alpha$  particle and the  $^{15}\text{N}$  core. The ground state of the nucleus  $^{15}\text{N}$  can be described as  $^{16}\text{O}$  with a hole in the  $p_{1/2}$  shell.

The cluster wave function  $u_{NLJ}(r)$  which describes the relative motion of the  $\alpha$  particle and the  $^{15}\text{N}$  core is characterized by the node number  $N$  and the orbital and total angular momenta  $L$  and  $J$  with  $J = L \pm 1/2$ . The cluster  $N$  and  $L$  values are related to the corresponding quantum numbers  $n_i$  and  $l_i$  of the four nucleons forming the  $\alpha$  cluster in the  $sd$  shell:

$$Q = 2N + L = \sum_{i=1}^4 (2n_i + l_i) = \sum_{i=1}^4 q_i \quad (3)$$

For  $^{20}\text{Ne}$  one expects five cluster states with positive parity for the ground state band ( $Q = 8, J^\pi = 0^+, 2^+, 4^+, 6^+, 8^+$ ) and five cluster states with negative parity ( $Q = 9, J^\pi = 1^-, 3^-, 5^-, 7^-, 9^-$ ). The coupling of these bands with the ground state spin of  $^{15}\text{N}$  ( $J^\pi = 1/2^-$ ) leads to close doublets in  $^{19}\text{F}$  because of a weak spin-orbit coupling (with the exception of the  $L = 0, J^\pi = 1/2^-$  state which cannot be split into a doublet).

The properties of these bands have been discussed in detail in [30, 31, 32, 33] (and references therein). In the following we shall focus our interest on the  $Q = 9, L = 1, J^\pi = 1/2^+, 3/2^+$  doublet which appears as resonances in the  $^{15}\text{N}(\alpha, \gamma)^{19}\text{F}$  reaction at  $E_x = 5337$  keV and 5501 keV.

Following the procedure outlined in [30, 34] we tried to describe these resonances as so-called potential resonances. A full discussion of potential resonances is also given in [35]. Our analysis uses systematic folding potentials which have been shown to describe many properties of the systems  $^{15}\text{N} \otimes \alpha$  and  $^{16}\text{O} \otimes \alpha$  [30] including a weak spin-orbit potential with a shape  $\sim 1/r dV/dr$ . The strength of the central potential has been adjusted to reproduce the properly weighted average energy of the  $L = 1$  doublet, and the strength of the spin-orbit potential was adjusted to the energy difference between both states. A similar procedure was performed for  $L = \text{even}$  partial waves. One finds similar normalization parameters of the folding potential of  $\lambda \approx 1.3$  for even and odd partial waves. After this adjustment the potential is fixed, and the elastic scattering wave function can be calculated without any further adjustment. One finds a good agreement with the experimentally measured excitation functions of elastic scattering which were already shown in Fig. 3. However, the widths of both resonances are slightly overestimated. For the  $1/2^+$  state at  $E_x = 5337$  keV we find  $\Gamma_\alpha^{\text{calc}} = 3.44$  keV compared to  $\Gamma_\alpha^{\text{exp}} = 1.3 \pm 0.5$  keV (from this work), and for the  $3/2^+$  state at  $E_x = 5501$  keV we find  $\Gamma_\alpha^{\text{calc}} = 9.99$  keV compared to  $\Gamma_\alpha^{\text{exp}} = 4.2 \pm 0.9$  keV (weighted average of the adopted value and this work). In both cases  $\Gamma_\alpha^{\text{exp}} \approx 0.4 \times \Gamma_\alpha^{\text{calc}}$  which shows that the wave functions of both resonances consist of about 40%  $\alpha$  cluster contribution. Reduced widths have been calculated for these states leading to  $\theta_\alpha^2 = 0.53$  and 0.52 for the  $E_x = 5337$  keV state from the generator coordinate method (GCM) [32] and from the orthogonality condition model (OCM) [36]

and to  $\theta_\alpha^2 = 0.46$  and 0.50 for the  $E_x = 5501$  keV state. A similar result is also obtained for the  $L = 1, J^\pi = 1^-$  resonance in  $^{20}\text{Ne}$  (see Fig. 10 of [30]).

From the wave functions of the potential model the direct capture (DC) cross section can be calculated in the  $E_x = 5337$  keV and 5501 keV resonances and at lower and higher energies. The full formalism has been described in [34]. The calculated DC cross section for the transition to the  $E_x = 110$  keV state is compared to experimental data in Fig. 4. The spectroscopic factor of the final state has been taken from [36]. Note that the  $E_x = 110$  keV state is the lowest  $\alpha$  cluster state in  $^{19}\text{F}$  with  $Q = 8, N = 4, L = 0$ , and  $J^\pi = 1/2^-$ . Good agreement is found in the resonances and in a broad energy interval at lower and higher energies. Similar results have been obtained for the transitions to the  $\alpha$  cluster states with  $L = 2$  and  $J^\pi = 5/2^-$  at  $E_x = 1346$  keV and  $J^\pi = 3/2^-$  at  $E_x = 1459$  keV. Especially, the relatively small cross section of the transition  $J^\pi = 3/2^+, E_x = 5501$  keV  $\rightarrow J^\pi = 3/2^-, E_x = 1459$  keV (see Table II) is also reproduced by the DC calculations.

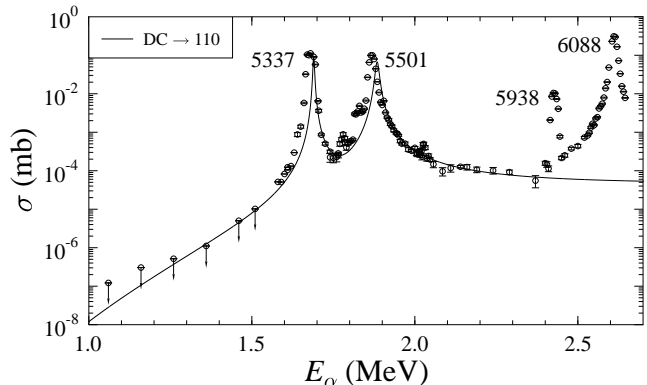


FIG. 4: The calculated direct capture cross section for the transition to the first excited state with  $J^\pi = 1/2^-$  at  $E_x = 110$  keV is compared to experimental data. One finds good agreement between experiment and theory in the  $J^\pi = 1/2^+$  and  $3/2^+$  resonances at  $E_x = 5337$  keV and 5501 keV and in a broad energy interval at lower and higher energies.

If the energy differs sufficiently from the resonance energy, the calculated cross section depends only weakly on the energy. However, this “direct capture” results from the tail of the  $E_x = 5337$  keV and 5501 keV resonances; the experimental proof is the identical branching ratio which is observed in the  $E_x = 5501$  keV resonance and in the whole energy range from 5400 keV  $\lesssim E_x \lesssim$  5700 keV (of course, excluding the narrow resonances at  $E_x = 5418$  keV, 5464 keV, 5535 keV, and 5621 keV).

## V. ASTROPHYSICAL REACTION RATE

The astrophysical reaction rate of  $^{15}\text{N}(\alpha, \gamma)^{19}\text{F}$  is dominated by resonant contributions. In total, 48 resonances have been taken into account in the NACRE compilation

[19]. For the most important low-lying resonances the strengths from a transfer experiment [20] were adopted, and our results from a first analysis of our experimental data [37] were taken into account. In cases where several determinations of the resonance strength were available the weighted average has been adopted which is close to our values because of our small experimental uncertainties. Because the resonance strengths in this work are identical to [37] the adopted reaction rate of [19] does not change.

The influence of the various resonances to the astrophysical reaction rate is shown in Fig. 5. The total reaction rate has been taken from the fit function provided by the NACRE compilation [19]. The contribution of each resonance has been calculated using the strengths from Table I and the formalism for narrow resonances.

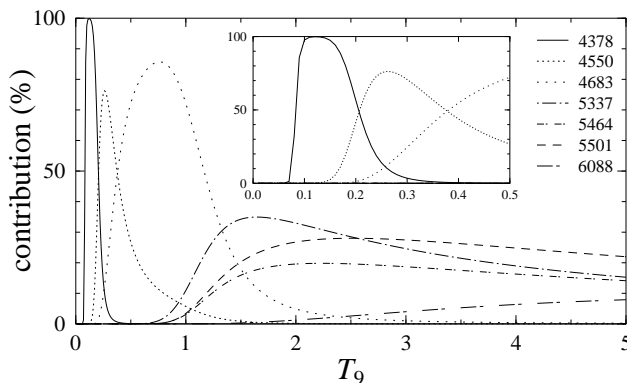


FIG. 5: Contribution of seven individual resonances to the total reaction rate  $N_A \langle \sigma v \rangle$  of the reaction  $^{15}\text{N}(\alpha, \gamma)^{19}\text{F}$  in per cent. The inset shows the low temperature region ( $T_9 \leq 0.5$ ). Below  $T_9 \lesssim 1.2$  the reaction rate is dominated by three individual resonances at  $E_x = 4378, 4550,$  and  $4683$  keV. At higher temperatures the reaction rate is given by the sum of several strong resonances.

Below  $T_9 = 0.08$  direct capture becomes relevant [20]; however, the absolute reaction rate at  $T_9 = 0.08$  drops below  $N_A \langle \sigma v \rangle = 10^{-25} \text{ cm}^3 \text{ s}^{-1} \text{ mole}^{-1}$  which is considered as negligible in usual astrophysical calculations [19].

At  $0.1 \leq T_9 \leq 0.2$  the reaction rate is completely determined by the  $7/2^+$  state at 4378 keV. Therefore the uncertainty of the reaction rate is given by the uncertainty of this resonance strength which is a factor of two [20].

The uncertainty of the reaction rate is significantly reduced at higher temperatures by the reduced experimental uncertainties of this work. In the temperature interval  $0.2 \lesssim T_9 \lesssim 0.4$  the  $5/2^+$  resonance at 4550 keV is dominating, and the interval  $0.4 \lesssim T_9 \lesssim 1.2$  is governed by the  $5/2^-$  resonance at 4683 keV. Above  $T_9 \gtrsim 1.2$  several strong resonances are contributing to the reaction

rate with typical contributions of the order of 10% – 30%. The experimental uncertainties for these resonance strengths of about 10% lead to an experimentally determined reaction rate with similar uncertainty [19]. Because of the relatively high excitation energy of the first excited state in  $^{15}\text{N}$ , the reaction rate which is calculated from laboratory data, is identical to the reaction rate under stellar conditions [19].

## VI. CONCLUSIONS

We have measured 14 resonances of the reaction  $^{15}\text{N}(\alpha, \gamma)^{19}\text{F}$  at low energies between  $0.6 \text{ MeV} \leq E_\alpha \leq 2.7 \text{ MeV}$ . The combination of the DYNAMITRON high-current accelerator, the windowless gas target RHINOCEROS, and large HPGe detectors with active shieldings leads to the excellent sensitivity of the experimental set-up.

Two resonances have been detected for the first time in the  $(\alpha, \gamma)$  channel. The uncertainties of the resonance strengths are reduced significantly. Branching ratios could be determined with improved precision; roughly 20 new weak branchings were seen for the first time. Typical detection limits are of the order of  $1 \mu\text{eV}$  for resonance strengths and far below 1% for weak branching ratios. Additionally, partial widths  $\Gamma_\alpha$  and  $\Gamma_\gamma$  were derived from the combination of experimental resonance strengths and measured ratios  $\Gamma_\gamma/\Gamma$  [24].

The states at  $E_x = 5337$  keV and 5501 keV have been identified unambiguously as the  $L = 1, J^\pi = 1/2^+$  and  $3/2^+$  doublet of  $^{15}\text{N} \otimes \alpha$  cluster states. This identification is based on the large partial widths  $\Gamma_\alpha$ , the angular distribution of elastic scattering, and the decay branchings of these states. The analysis of the yield curves over a broad energy interval has allowed to determine the total width of the  $E_x = 5337$  keV state for the first time and to confirm the total width of the  $E_x = 5501$  keV state. For both levels we find reduced widths  $\theta_\alpha^2 \approx 0.4$  in good agreement with various theoretical predictions.

The astrophysical reaction rate of the NACRE compilation [19] remains unchanged. The resonance strengths in this work are identical to our previous analysis [37] which has been taken into account in [19]. The uncertainties of the reaction rate have been reduced significantly at temperatures above  $T_9 = 0.2$ .

## Acknowledgments

We thank U. Kneissl for supporting this experiment. The help of R. Kunz, A. Mayer, and the DYNAMITRON crew during the beamtimes is gratefully acknowledged. This work was supported by Deutsche Forschungsgemeinschaft DFG (Sta290).



- 
- [1] M. Forestini, S. Goriely, A. Jorissen, and M. Arnould, *Astron. Astroph.* **261**, 157 (1992).
- [2] A. Jorissen, V. V. Smith, and D. L. Lambert, *Astron. Astroph.* **261**, 164 (1992).
- [3] G. Meynet and M. Arnould, *Astron. Astroph.* **355**, 176 (2000).
- [4] S. E. Woosley, D. H. Hartmann, R. D. Hoffman, and W. C. Haxton, *Astrophys. J.* **356**, 272 (1990).
- [5] Görres, J., in *Nuclei in the Cosmos VII*, edited by S. Kubono *et al.* (2002).
- [6] R. K. Wallace and S. E. Woosley, *Astrophys. J. Suppl.* **45**, 389 (1981).
- [7] K. Langanke, M. Wiescher, W. A. Fowler, and J. Görres, *Astrophys. J.* **301**, 629 (1986).
- [8] Y. M. Butt, J. W. Hammer, M. Jaeger, R. Kunz, A. Mayer, P. D. Parker, R. Schreiter, and G. Staudt, *Phys. Rev. C* **58**, R10 (1998).
- [9] F. deOliveira, A. Coc, P. Aguer, G. Bogaert, J. Kiener, A. Lefebvre, V. Tatischeff, J.-P. Thibaud, S. Fortier, J. M. Maison, *et al.*, *Phys. Rev. C* **55**, 3149 (1997).
- [10] P. V. Magnus, M. S. Smith, P. D. Parker, R. E. Azuma, C. Campbell, J. D. King, and J. Vise, *Nucl. Phys. A* **470**, 206 (1987).
- [11] D. W. O. Rogers, J. H. Aitken, and A. E. Litherland, *Can. J. Phys.* **50**, 268 (1972).
- [12] D. W. O. Rogers, R. P. Beukens, and W. T. Diamond, *Can. J. Phys.* **50**, 2428 (1972).
- [13] W. R. Dixon and R. S. Storey, *Can. J. Phys.* **49**, 1714 (1971).
- [14] W. R. Dixon, R. S. Storey, J. H. Aitken, A. E. Litherland, and D. W. O. Rogers, *Phys. Rev. Lett.* **27**, 1460 (1971).
- [15] J. H. Aitken, R. E. Azuma, A. E. Litherland, A. M. Charlesworth, D. W. O. Rogers, and J. J. Simpson, *Can. J. Phys.* **48**, 1617 (1970).
- [16] P. C. Price, *Proc. Phys. Soc. (London) A* **70**, 661 (1957).
- [17] F. Ajzenberg-Selove, *Nucl. Phys. A* **475**, 1 (1987).
- [18] D. R. Tilley, H. R. Weller, C. M. Cheves, and R. M. Chasteler, *Nucl. Phys. A* **595**, 1 (1995).
- [19] C. Angulo, M. Arnould, M. Rayet, P. Descouvemont, D. Baye, C. Leclercq-Willain, A. Coc, S. Barhoumi, P. Aguer, C. Rolfs, *et al.*, *Nucl. Phys. A* **656**, 1 (1999).
- [20] F. de Oliveira, A. Coc, P. Aguer, C. Angulo, G. Bogaert, J. Kiener, A. Lefebvre, V. Tatischeff, J.-P. Thibaud, S. Fortier, *et al.*, *Nucl. Phys. A* **597**, 231 (1996).
- [21] J. W. Hammer, *Tech. Rep.*, Institut für Strahlenphysik, Universität Stuttgart (1999).
- [22] V. Kölle, U. Kölle, S. E. Braitmayr, P. Mohr, S. Wilmes, G. Staudt, J. W. Hammer, M. Jaeger, H. Knee, R. Kunz, *et al.*, *Nucl. Inst. Meth. Phys. Res. A* **431**, 160 (1999).
- [23] S. Wilmes, Ph.D. thesis, Universität Tübingen (1996).
- [24] D. M. Pringle and W. J. Vermeer, *Nucl. Phys. A* **499**, 117 (1989).
- [25] J. F. Ziegler, *Helium Stopping Powers and Ranges in All Elements* (Pergamon Press, New York, 1977).
- [26] F. Ajzenberg-Selove, *Nucl. Phys. A* **190**, 1 (1972).
- [27] S. Wilmes, P. Mohr, U. Atzrott, V. Kölle, G. Staudt, A. Mayer, and J. W. Hammer, *Phys. Rev. C* **52**, R2823 (1995).
- [28] Á. Z. Kiss, B. Nyakó, E. Somorjai, A. Antilla, and M. Bister, *Nucl. Inst. Meth. Phys. Res. A* **203**, 107 (1982).
- [29] P. M. Endt, *At. Data Nucl. Data Tables* **23**, 3 (1979).
- [30] H. Abele and G. Staudt, *Phys. Rev. C* **47**, 742 (1993).
- [31] B. Buck and A. A. Pilt, *Nucl. Phys. A* **280**, 133 (1977).
- [32] P. Descouvemont and D. Baye, *Nucl. Phys. A* **463**, 629 (1987).
- [33] M. Dufour and P. Descouvemont, *Nucl. Phys. A* **672**, 153 (2000).
- [34] P. Mohr, V. Kölle, S. Wilmes, U. Atzrott, G. Staudt, J. W. Hammer, H. Krauss, and H. Oberhummer, *Phys. Rev. C* **50**, 1543 (1994).
- [35] P. Mohr, H. Beer, H. Oberhummer, and G. Staudt, *Phys. Rev. C* **58**, 932 (1998).
- [36] T. Sakuda and F. Nemoto, *Prog. Theor. Phys.* **62**, 1606 (1979).
- [37] S. Wilmes, V. Kölle, U. Kölle, G. Staudt, P. Mohr, J. W. Hammer, and A. Mayer, *Nucl. Phys. A* **621**, 145c (1997).